PHYSICAL REVIEW D VOLUME 21, NUMBER 1 1 JANUARY 1980

Angular distributions of heavy-quark jets in e^+e^- annihilation

G. Grunberg
Laboratory of Nuclear Studies, Cornell University, Ithaca, New York 14853
and Departement de Physique Mathematique, USTL, 34060 Montpellier Cedex, France*

Yee Jack Ng
Institute of Field Physics, Department of Physics and Astronomy, University of North Carolina, Chapel Hill, North Carolina 27514

S.-H. H. Tye
Laboratory of Nuclear Studies, Cornell University, Ithaca, New York 14853
(Received 30 May 1979)

We propose that the angular distribution of heavy-quark jet production in e^+e^- annihilation is a clean place to measure the quark mass (e.g., accurate to within a few percent for the b quark) in perturbative quantum chromodynamics (QCD). We present our argument as to why this is the case (as compared to measurements given by the total cross section). We also evaluate the leading-order perturbative QCD correction to the angular distribution; we find that the QCD effect on the angular distribution is small except when the velocity v is close to one. Our formula gives the leading QCD correction to the angular distribution of hadronic jets, with the quark-mass effects fully taken into account.

I. INTRODUCTION

There has been a great deal of interest recently in the study of quantum chromodynamics (QCD), which involves the interactions of quark and gluon fields. This field theory has been used to calculate many physically interesting quantities, and confrontation with experiments looks very encouraging.

The only free parameters of QCD are the color coupling $\alpha_c = g^2/4\pi$ and the quark masses m_i where $i = 1, 2, \ldots, N$ for N number of flavor. It goes without saying that determination of the above parameters is of great importance. In this work, we discuss in detail one method to measure the heavy-quark mass. We shall first point out the method; then we shall discuss some of the issues that accompany our approach, namely, (1) the sensitivity of the experiment, (2) confinement effects,[1] (3) definition of the quark mass, and (4) higher-order perturbative QCD corrections. We believe all these complications can be handled easily, and the method we propose is a very clean and accurate way to measure heavy-quark masses. We estimate that our method can determine the mass of the b quark, e.g., to within ~0.3 GeV, i.e., to ~6% accuracy.

The idea is both obvious and trivial. Consider e^+e^- annihilation into a heavy-quark pair $(q_i\bar{q}_i)$ in lowest order,

$$\frac{d\sigma_i(s)}{d\cos\theta} = \frac{3\alpha^2\pi e_i^2}{2s}\frac{v}{2}\left[(3-v^2)(1+\cos^2\theta) + (1-v^2)(1-3\cos^2\theta)\right], \quad (1.1)$$

where θ is the angle between the quark and the electron direction, s is the c.m. energy (W) squared, $s = W^2$, v is the velocity of the quark with mass m_i,

$$v^2 = 1 - \frac{4m_i^2}{s} \equiv 1 - \xi\,, \quad (1.2)$$

and e_i is the electrical charge of the quark measured in units of $(4\pi\alpha)^{1/2}$. Rewriting Eq. (1.1) for later convenience, we have

$$\frac{1}{\sigma_0}\frac{d\sigma_i}{d\cos\theta} = \tfrac{3}{8}(2-v^2)v[1+B_0(v)\cos^2\theta]\,, \quad (1.3a)$$

where

$$B_0(v) = \frac{v^2}{2-v^2}\,. \quad (1.3b)$$

$\sigma_0 = (4\pi\alpha^2/s)e_i^2$ is the total cross section $e^+e^- \to q_i\bar{q}_i$ in the limit $4m_i^2/s \to 0$. Hence we see that the angular distribution of the quark pair deviates from $(1+\cos^2\theta)$ when the quark-mass effect is included. To see how much this deviation is, let us consider the charmed quark. Its mass quoted in the literature ranges from 1.1 to 1.85 GeV.[2] The coefficient $B_0(m, s)$ is plotted in Fig. 1, which illustrates clearly the dependence of B_0 on the quark mass. For example,

$$\frac{B_0(m = 1.1\ \text{GeV},\ W = 7\ \text{GeV})}{B_0(m = 1.85\ \text{GeV},\ W = 7\ \text{GeV})} \sim 1.5\,.$$

This means a good measurement of the angular distribution of the charmed-quark production can certainly give an accurate value (i.e., to within 10–20%) of the charmed-quark mass. The coefficient $B_0(m, s)$ is also shown for the b-quark case in Fig. 1, where we have taken the b-quark mass to be (i) 4.2 and (ii) 5.5 GeV.

An immediate question concerning our suggestion should arise: The total cross section for the production of heavy-quark pair $\sigma_{tot}(m, s)$ also depends on the quark mass m and s; why then don't we use the measurement of σ_{tot}, or equivalently, its contribution to R, to derive the value of m_i? If this is not possible, then why does the angular distribution allow us to obtain the value of m_i? Let us present our argument in some detail.

That $\sigma_{tot}(m, s)$ does not provide a measurement of the quark mass has been discussed in the literature.[3] In every order of perturbative QCD, the theory predicts the production of quarks and gluons, whereas only color-singlet bound states of quarks and gluons (i.e., hadrons) have been observed in nature so far. This means that direct application of perturbative QCD to calculate physical quantities is in general not justified. Since the phenomenon of quark confinement in QCD is not yet understood, all sensible application of perturbative QCD must be free from confinement (i.e., long-range) effects. The process $e^+e^- \to q_i\bar{q}_i$ has a threshold at $s = 4m_i^2$ in perturbative QCD whereas nature puts the threshold at $s = 4m_H^2$ where H is the lightest meson containing q_i or $\bar{q}_i$. Excluding pure coincidence, $m_H \neq m_i$. Hence a direct application of perturbative QCD is meaningless. Also (naive) perturbative QCD predicts Coulombic bound states ($q\bar{q}$) in the e^+e^- channel while observed bound states clearly do not obey a Coulombic binding. Hence, to obtain a meaningful comparison between theory and experiment, we must render the calculation infrared insensitive. One way is to smear the perturbative QCD cross section in s, as suggested by Poggio, Quinn, and Weinberg.[3] However, in the process of smearing, one (deliberately) washes out the distinction between contributions from the quark-antiquark and multigluon production (or quark-antiquark bound states) and the actual production of hadrons. Thus the smearing also washes out any (precise) meaning to the mass parameter in σ_{tot}.

There have been other attempts[4] to extract the values of the quark masses from σ_{tot}. One of the methods uses finite-energy sum rules and the notion of duality and relies heavily on the resonances in σ_{tot} measurements. The quark-mass value obtained this way is closer to the "constituent quark mass" value than to the quark mass that appears in the Lagrangian, which is what we are suggesting to measure. (See Sec. II for more discussions.)

Now we would like to argue that, under appropriate smearing, the angular distribution of the heavy-quark–antiquark production is determined by perturbative QCD, and the quark mass here is physically meaningful, in contrast to the case of σ_{tot}. We do not have a rigorous justification for this procedure; however, it is supported by the following simple intuitive argument, which seems to us to be quite plausible. In any case, the point in question can be cleanly tested experimentally.

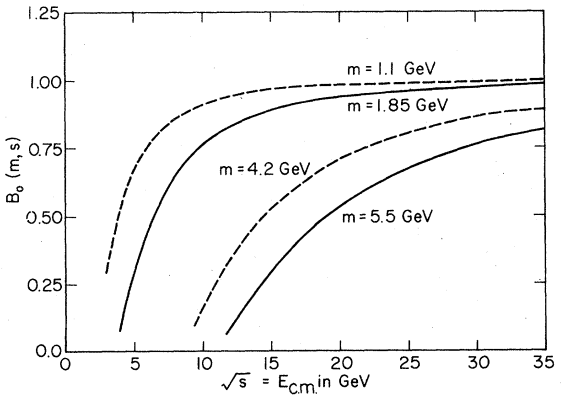

FIG. 1. The lowest-order coefficient $B_0(v) = B_0(m, s)$ in the angular distribution $[1 + B_0(v)\cos^2\theta]$ as a function of the total energy in the center-of-mass frame in e^+e^- annihilation. For the purpose of illustration, we have chosen 1.1 and 1.85 GeV for the charmed-quark mass, and 4.2 and 5.5 GeV for the b-quark mass.

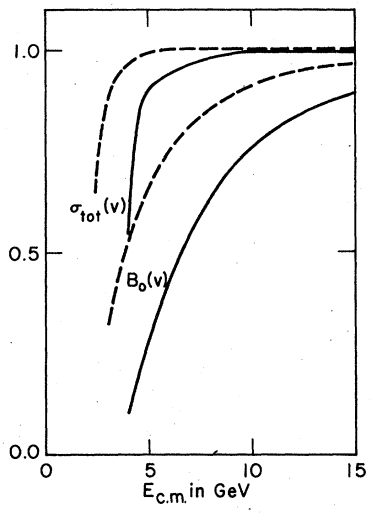

FIG. 2. The top two curves are $\sigma_{tot}(m, s)/\sigma_{tot}(o, s)$. The lower two curves are the coefficient B_0 taken from Fig. 1. The dashed curves are for mass = 1.1 GeV. The solid curves are for mass = 1.85 GeV.

Our argument is best illustrated in Fig. 2. We observe that the cross section approaches its asymptotic value [i.e., $\sigma_{\text{tot}}(m=0, s)$] much faster than the coefficient $B_0(m, s)$ as the total energy increases. Now for the cross section, we can trust the perturbative QCD calculations only for energies far above the continuum threshold. However, at those energies, the cross section has already reached its asymptotic value. This means any quark-mass effect is negligible. The situation for the angular distribution is quite different. Because $B_0(m, s)$ approaches its asymptotic value much slower than σ_{tot}, the angular distribution still depends strongly on the value of the quark mass even at energies way above the continuum threshold. This also means that at the energy range where $B(m, s)$ is to be measured, one has essentially the maximum cross section available. As we shall show, this feature persists when perturbative QCD corrections are included.

To measure $B(m, s)$, it is important to go to energies way above the continuum threshold. To see this explicitly, let us take $m_H > m_t$ and consider three regions of s.

(i) $4m_H^2 > s > 4m_t^2$. As mentioned earlier, this region clearly demonstrates that σ_{tot} is strongly dependent on confinement effects since $\sigma_{\text{tot}}(\text{perturbative QCD}) \neq 0$ while $\sigma_{\text{tot}}(e^+e^- \to H + \bar{H} + X) = 0$. Hence it is meaningless to talk about the angular distribution in this energy range.

(ii) $s \gtrsim 4m_H^2$. H is taken to be a pseudoscalar meson, the lightest meson containing the heavy quark. Then the angular distribution of the exclusive process $e^+e^- \to H\bar{H}$ is dictated by the vector-scalar-scalar coupling. This completely dictates the form of the angular distribution so the underlying photon-quark-antiquark coupling is totally masked. To avoid this situation, we must take $s \gg 4m_H^2$.

(iii) $s \gg 4m_H^2$ such that e^+e^- annihilation can go to *either* one of the many different channels of a pair of excited H' exclusively *or* a multiparticle final state where one of the particles contains the heavy quark, another the heavy antiquark. Although the individual exclusive channel $e^+e^- \to H + \bar{H}$ has an angular distribution dictated by spin properties of H, it may be possible that if we smear over many exclusive channels, the energy-averaged angular distribution reflects the underlying quark structure.

Fortunately, for heavy quarks, the mass spacings between H and its excited states are expected to be very small, while the hadronic width of an excited state is expected in general to be quite large and is increasing as $m_{H'}$ increases. Hence, smearing can be done over small regions of $\sqrt{s}$, since the large widths of the excited H's provide a built-in smearing already.

To be concrete, consider the charmed-quark case. When we are close to the threshold, we must smear over a large region in s. But for $s > 4m_H^2$, say (for charm) $\sqrt{s} > 5$ GeV, the size of the smearing can be taken to be quite small, say $\Delta s \lesssim 1$ GeV^2. This is because the $(q\bar{q})$ states in the e^+e^- channel are resonances as s is above the continuum threshold. The density of such resonances and their individual widths increase as a function of s. This automatically smoothes the cross section $e^+e^- \to q\bar{q} \to$ hadrons. In Fig. 2, we have plotted the zeroth order $\sigma_{\text{tot}}(m, s)$ normalized with $\sigma_0 = \sigma_{\text{tot}}(m=0, s)$ for the two quark masses $m = 1.1$ and 1.85 GeV. For $\sqrt{s}$ above 5 GeV, the difference between the two cross sections (before smearing) is tiny, while the difference between their angular distribution is still substantial. After smearing, we expect the difference in σ_{tot} would be washed out, but the difference in the angular distribution will remain substantial. This allows the measurement of the quark mass from angular distribution but not from σ_{tot}.

The physical picture for e^+e^- annihilation is as follows: The virtual photon goes into a heavy-quark–antiquark pair in a certain direction. The quark and antiquark start to fragment along that direction (in the language of duality, fragmentation means that a pair of highly excited hadrons are created, which then decay strongly into lighter hadrons). Since fragmentation comes from confinement effects, which are soft in nature, the direction of the initial quark pair would be maintained during fragmentation.

Since we can use our method to measure masses of quarks of different flavors (i.e., we can separate quarks of different flavors) it suffices to use again the charmed-quark case for illustration. In that case we look for D, D^* mesons. From the decay modes (e.g., $K^+\pi^-\pi^+$ mode) we can reconstruct the energy and direction of the D or D^* meson and hence the direction for the initial charmed quark. We can check this by looking at the jet axis of such events. Confinement effects give a transverse momentum spread of the order of 300 MeV. At $\sqrt{s} = 10$ GeV for example, the angular deviation due to confinement is of the order of a few degrees. Hence we should smear θ over, say $\Delta\theta \sim 5°$.

Alternatively we can select the $c\bar{c}$ events by a analysis of jetlike properties. In the energy range of $E_{e^+e^-} = 4$ to 8 GeV, we expect the $c\bar{c}$ events to be less jetlike than the light-quark events. An analysis of large-transverse-momentum (with respect to the jet axis) events should help the selection of $c\bar{c}$ events. The two ways of selecting $c\bar{c}$ events can be used simultaneously.

In principle, the QCD coupling and the quark

mass determine both ΔR due to the quark pair and the jet angular distribution. This provides a test of the mass dependence of (zeroth- plus first-order) QCD in e^+e^- annihilation. Once this is verified, it can be used to measure quark masses. Angular distribution measured at different energies can substantially improve the accuracy of the mass determination. If neutral particles as well as charged particles are detected and measured, the jet axis, and hence the jet angular distribution, can be determined more accurately. If the coefficient B at a fixed energy has an error of 0.1, we expect the charmed-quark mass to be determined to within 0.1–0.2 GeV, and the b-quark mass to within 0.3 GeV.

Of course, once the quark masses are known (either using this method or some other methods), the jet angular distribution for all hadronic events is simply given by a sum over all flavors of the jet angular-distribution formula we give in Sec. III.

There are two other important points that we shall discuss. First, what do we mean by the quark mass? This is discussed in Sec. II, which is essentially a review of what is known in the literature. We include it not because we have something new to say, but rather that a proposal of quark-mass measurement would be incomplete without a discussion of what we mean by the mass of a quark. The other point, which is our main work in this paper, is the evaluation of the nontrivial leading-order perturbative QCD correction to the production of heavy quarks (see Fig. 3). The physical results are summarized in Sec. III, where a discussion of the physics is also included. Details of the calculation are contained in Sec. IV and the Appendix. The inclusion of the QCD effect is important, since even in the zero-quark-mass-limit, the deviation of the angular distribution from $(1+\cos^2\theta)$ due to QCD corrections is of the order of 10 to 20% (see Sec. III), which is comparable to the effect we want to measure. However, we find that the QCD correction to the angular distribution is small (~3%) except for the velocity v close to its upper ($v=1$, i.e., $m_i \to 0$ or $s \to \infty$) or its lower ($v=0$, i.e., close to the threshold region) limits. (See Sec. III.)

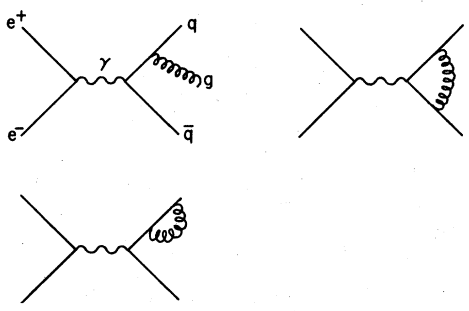

FIG. 3. The leading QCD contributions to the $e^+e^- \to \bar{q}q$ process.

For small velocities, the perturbative expansion is not valid (see Sec. III for more discussion on this point); for velocity close to unity, the angular-distribution deviation is essentially proportional to the strong-interaction coupling α_s. We calculate the angular distribution for both the cross section and the energy-weighted cross section to leading order in α_s (they are identical in the zeroth order). We do not know which is an easier quantity to measure experimentally.

II. THE QUARK MASS

Since quarks are not free, we have to be precise in what we mean by quark masses. For light quarks, it is natural to consider the current quark masses that occur in the divergence of the chiral flavor $SU(N)\times SU(N)$ currents. In particular, the axial current for flavor f gives

$$\partial_\mu J^\mu_{5f} = i\left[Q_{5f}, \sum_j m_j \bar{\psi}_j \psi_j\right],$$

where the quark masses are those that occur in the strong interaction Lagrangian. Chiral symmetry and other considerations determine the light-quark masses.[5] Unfortunately we cannot extend this method to the determination of the heavy-quark masses.

Although quarks are confined so that we cannot measure the quark masses by letting the quarks go on mass shell, we can still define the quark mass to be the location of the pole in the quark propagator. We can carry out the mass renormalization so that to any given order in perturbative QCD, the quark propagator has a pole at $\not{p}=m$. This definition need not imply the existence of free quarks. Experience from two-dimensional QCD[6] suggests that the following intriguing possibility may take place. The hadron-quark vertex $\Gamma(p_i)$ always develops a zero as any of the quark propagators approaches its mass shell (see Fig. 4),

$$\Gamma(p_1, p_2, p_3) \xrightarrow{p_j \to m_j} 0 \quad \text{for any } j,$$

such that the amplitude for a free-quark production is always suppressed.

An alternative defintion has been suggested by

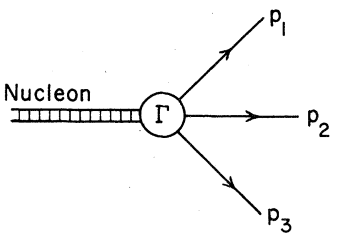

FIG. 4. The hadron-quark vertex $\Gamma(p_1,p_2,p_3)$. The solid lines are quarks.

Georgi and Politzer.[7] In their approach, one carries out the wave-function and coupling-constant renormalization at momentum p such that $p^2=-\mu^2$. The quark mass is then given by the inverse quark propagator

$$\Gamma_2^{\text{renormalized}}|_{p^2=-\mu^2}=\not{p}-m\,.$$

With the use of the renormalization-group equation, the mass behaves like a running parameter, very similar to the color coupling g; that is, they have different effective values at different energy-momentum Q involved:

$$\frac{\partial\bar{g}}{\partial t}=\beta_g(\bar{g},\bar{m}/Q)\,, \tag{2.1a}$$

$$\frac{\partial\bar{m}}{\partial t}=\bar{m}\gamma_m(\bar{g},\bar{m}/Q)\,, \tag{2.1b}$$

where $t=\frac{1}{2}\ln(Q^2/\mu^2)$. To lowest nontrivial order in QCD,

$$\beta_g=\frac{-g^3}{16\pi^2}\left\{11-\tfrac{2}{3}\sum_i\left[1-\frac{6m_i^2}{\mu^2}+\frac{12m_i^4/\mu^4}{(1+4m_i^2/\mu^2)^{1/2}}\ln\left(\frac{(1+4m_i^2/\mu^2)^{1/2}+1}{(1+4m_i^2/\mu^2)^{1/2}-1}\right)\right]\right\}, \tag{2.2a}$$

$$\gamma_{m_i}=-\frac{8g^2}{16\pi^2}\left[1-\frac{m_i^2}{\mu^2}\ln\left(1+\frac{\mu^2}{m_i^2}\right)\right]. \tag{2.2b}$$

For the heavy-quark case, the angular distribution in Eq. (1.3) would be modified if we replace a fixed mass m by a running mass $\bar{m}(t)$. If we normalize $\bar{\alpha}_c(t=0)=0.3$ and $\bar{m}(t=0)=m=\mu/2$, then, using Eqs. (2.1) and (2.2), we obtain $B_0(v)\to B_m(v)$, where v is the velocity defined in Eq. (1.2). In Fig. 5, we compare the coefficient $B_m(v)$ with running mass to $B_0(v)$ given in Eq. (1.3). We find the deviation is small.

In the rest of this work, we shall use the "location of the pole" definition. Readers who are interested in the "running mass" definition can easily incorporate the effective-mass correction into the angular distribution by using Fig. 5.

For any given quark, the mass measured from the angular distribution should also be the mass that appears in deep-inelastic lepton-hadron scatterings and in weak decays. In deep-inelastic scatterings, the production of heavy quarks is, in general, small. Furthermore, this is complicated by the fact that the quark-mass effect occurs in a twist-four operator, and a complete treatment of all twist-four operators is required by gauge invariance. This renders the analysis complicated.

In principle, weak decays of heavy quarks also provide a means to measure the current quark masses. It would be interesting to compare the quark masses provided by that method with those measured by the "angular distribution" method which, we believe, is one of the cleanest ways to determine the heavy-quark masses.

Finally, it is well known that if the Higgs boson in weak and electromagnetic interactions is discovered, its decay into heavy-quark pairs should provide a clean way to determine the quark masses, since the strength of the quark–antiquark–Higgs-boson vertex is directly proportional to the quark mass. However, to use this method we have to wait for the discovery of the elusive Higgs bosons.

III. PERTURBATIVE QCD CORRECTION

In this section we will summarize our results of the leading-order QCD correction, the detailed

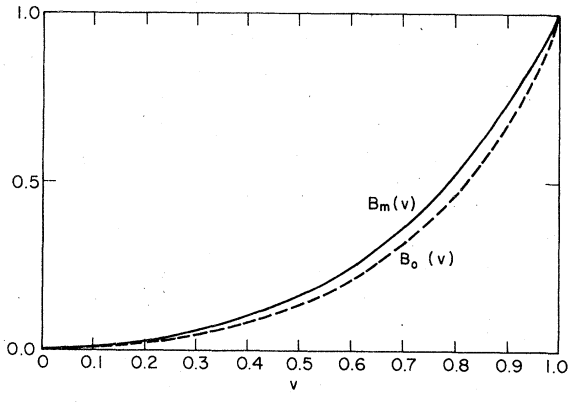

FIG. 5. The coefficients $B_0(v)$ and $B_m(v)$ as a function of the velocity v. $B_0(v)$ is given in Eq. (1.3); $B_m(v)$ is $B_0(v)$ modified with a running mass as defined by Eqs. (2.1) and (2.2).

calculation of which will be relegated to Sec. IV and the Appendix. The effect of perturbative QCD comes in when we consider the gluon-bremsstrahlung and radiative-correction diagrams shown in Fig. 3. For the massless-quark case, these diagrams have been studied in great detail.[8] The differential cross section for the gluon-bremsstrahlung diagrams is given by [recall $\sigma_0=(4\pi\alpha^2/s)e_i^2$]

$$\frac{1}{\sigma_0}\frac{d\sigma}{dx_1dx_2d\cos\theta_1}=\frac{\alpha_c}{4\pi}\left[\frac{x_1^2+x_2^2}{(1-x_1)(1-x_2)}(1+\cos^2\theta_1)+2\frac{(x_1+x_2-1)}{x_1^2}(1-3\cos^2\theta_1)\right], \tag{3.1}$$

where $x_i=2E_i/\sqrt{s}$, E_i is the energy of the final-state particles in the c.m. frame, $i=1,2,3$ for the quark, the antiquark, and the gluon, respectively, and θ_1 is the angle between the quark and the electron (we have taken $m_e=0$). For later use, we define $\tilde{\alpha}=C_2(R)\alpha_c=\frac{4}{3}\alpha_c$, where $C_2(R)$ is the value of the quadratic Casimir operator for the quark representation R = triplet, and $\alpha_c=g^2/4\pi$ is the strong-interaction coupling.

Since we are only interested in the angular distribution of the quark, we integrate over the x_i variables. Including the contributions from the radiative-correction diagram, we obtain, to leading order in α_c ($m_i=0$),

$$\frac{1}{\sigma_0}\frac{d\sigma}{d\cos\theta_1}=\frac{3}{8}\left(1+\frac{3}{4}\frac{\tilde{\alpha}}{\pi}\right)\left(1+\cos^2\theta_1+\frac{\tilde{\alpha}}{2\pi}(1-3\cos^2\theta_1)\right)$$

$$\propto 1+\left(1-\frac{2\tilde{\alpha}}{\pi}\right)\cos^2\theta_1. \tag{3.2}$$

All infrared divergences cancel exactly, as expected. For a typical value of $\tilde{\alpha}/\pi=0.1$, we have $1+0.8\cos^2\theta_1$. This deviation from $(1+\cos^2\theta)$ is comparable to that induced by the quark-mass effect. To include this effect in perturbative QCD, we must evaluate the diagrams in Fig. 3 with nonzero quark mass m.

The result of the differential cross section for the gluon-bremsstrahlung diagrams with quark mass m is given by

$$\frac{1}{\sigma_0}\frac{d\sigma}{dx_1dx_2d\cos\theta_1}=\frac{\alpha_c}{4\pi}\left[\tfrac{1}{8}\mathfrak{A}_1(1+\cos^2\theta_1)+(\tfrac{1}{8}\mathfrak{A}_2+\mathfrak{A}_3G)(1-3\cos^2\theta_1)\right], \tag{3.3}$$

where

$$\mathfrak{A}_1=\frac{8(x_1^2+x_2^2)}{(1-x_1)(1-x_2)}-4\xi\left(\frac{1}{(1-x_1)^2}+\frac{1}{(1-x_2)^2}+\frac{2}{1-x_1}+\frac{2}{1-x_2}\right)-2\xi^2\left(\frac{1}{1-x_1}+\frac{1}{1-x_2}\right)^2,$$

$$\mathfrak{A}_2=\frac{8\xi(x_1+x_2-1)}{(1-x_1)(1-x_2)}-2\xi^2\left(\frac{1}{1-x_1}+\frac{1}{1-x_2}\right)^2,$$

$$\mathfrak{A}_3=x_1+x_2-1-\frac{\xi(2-x_1-x_2)^2}{4(1-x_1)(1-x_2)},$$

$$G=\frac{2-2x_2-\xi(1-x_1)}{(1-x_2)(x_1^2-\xi)},$$

while in terms of the angle θ_3 (the angle between the gluon and the electron), it is given by

$$\frac{1}{\sigma_0}\frac{d\sigma}{dx_1dx_2d\cos\theta_3}=\frac{\alpha_c}{4\pi}\left[\tfrac{1}{8}\mathfrak{A}_1(1+\cos^2\theta_3)+(\tfrac{1}{8}\mathfrak{A}_2+\mathfrak{A}_3\mathfrak{C})(1-3\cos^2\theta_3)\right], \tag{3.4}$$

where

$$\mathfrak{C}=4(2-x_1-x_2)^{-2}-\xi(1-x_1)^{-1}(1-x_2)^{-1}.$$

Integrating over the angle θ, Eqs. (3.3) and (3.4) both give[9]

$$\frac{1}{\sigma_0}\frac{d\sigma}{dx_1dx_2}=\frac{2\alpha_c}{3\pi}\frac{\mathfrak{A}_1}{8}.$$

It is clear that the cross section (3.3) approaches the cross section (3.1) in the limit $m\to 0$. Integrating over the phase space in x_1, x_2, we obtain from Eq. (3.3), with the inclusion of radiative corrections,

$$\frac{1}{\sigma_0}\frac{d\sigma}{d\cos\theta_1}=\frac{3}{8}\left(1+\frac{\tilde{\alpha}}{\pi}P\right)\frac{v}{2}\left[(3-v^2)(1+\cos^2\theta_1)+\xi(1-3\cos^2\theta_1)\left(1+\frac{\tilde{\alpha}}{\pi}\mathfrak{W}\right)\right], \tag{3.5}$$

where ξ is defined in Eq. (1.2). P and $\mathfrak{W}$ are complicated functions of v to be given below. If we integrate over θ_1, the $(1-3\cos^2\theta_1)$ term integrates

to zero so that only the $(1+\cos^2\theta_1)$ term contributes to the total cross section:

$$\frac{\sigma}{\sigma_0}=\left(1+\frac{\tilde{\alpha}}{\pi}P(v)\right)\frac{v}{2}(3-v^2). \tag{3.6}$$

P has been calculated in the literature (see Sec. IV). An excellent interpolation formula (good to 1% throughout and exact as $v\to 0, 1$) has been suggested by Schwinger[10]:

$$P(v)\simeq\frac{\pi^2}{2v}-\frac{3+v}{4}\left(\frac{\pi^2}{2}-\frac{3}{4}\right). \tag{3.7}$$

Values of $vP(v)$ are given in Table I. The evaluation of $\mathfrak{w}(v)$ is more complicated. In terms of the Spence function

$$L(x)=-\int_0^x\frac{dt}{t}\ln|1-t|$$

it takes the form

$$v\mathfrak{w}\xi=\xi(1+\xi)\left[L\left(\frac{1+v}{2}\right)-L\left(\frac{1-v}{2}\right)\right]+v(1-3\xi)+\frac{(9+v^2)v\xi}{4(3-v^2)}+\frac{\mathfrak{M}}{2}$$
$$+\frac{\xi}{2}\ln\left(\frac{1+v}{1-v}\right)\left[(1+\xi)\left(\frac{4-\xi}{4}\right)+3-\xi-\frac{(4-\xi)^2}{4(2+\xi)}+\frac{3\xi-1}{\sqrt{\xi}}\ln\left(\frac{2+\sqrt{\xi}}{2-\sqrt{\xi}}\right)\right], \tag{3.8}$$

where

$$\mathfrak{M}=\mathfrak{M}_1(\sqrt{\xi},v)+\mathfrak{M}_1(-\sqrt{\xi},v),$$
$$\mathfrak{M}_1(\xi^{1/2},v)=[\sqrt{\xi}(3\xi-1)-\xi(1+\xi)]\left[L\left(\frac{1+v}{1+g^2}\right)-L\left(\frac{1-v}{1+g^2}\right)-L\left(\frac{1+v}{1-g^2}\right)+L\left(\frac{1-v}{1-g^2}\right)+L\left(\frac{g-v}{g+g^2}\right)-L\left(\frac{g+v}{g+g^2}\right)\right.$$
$$\left.-L\left(\frac{g-v}{g-g^2}\right)+L\left(\frac{g+v}{g-g^2}\right)-L\left(\frac{g-v}{1+g}\right)+L\left(\frac{g+v}{1+g}\right)+L\left(\frac{v-g}{1-g}\right)-L\left(-\frac{g+v}{1-g}\right)\right], \tag{3.9}$$

where

$$g^2=1-\sqrt{\xi}.$$

The function $\xi\mathfrak{w}(v)$ is finite for all values of v between 0 and 1 (see Fig. 6). $\mathfrak{w}(v)$ is small in comparison to $P(v)$ except at v close to 1. Values of $\xi\mathfrak{w}(v)$ are given in Table I.

The angular distribution of the heavy quark can be written in the following form to order α_c,

$$\frac{d\sigma}{d\cos\theta_1}\propto 1+B_1(v)\cos^2\theta_1,$$
$$B_1(v)=\frac{v^2}{2-v^2}\left[1-\frac{\tilde{\alpha}}{\pi}\xi\mathfrak{w}(v)\frac{3-v^2}{v^2(2-v^2)}\right]. \tag{3.10}$$

We note that $\xi\mathfrak{w}(v)|_{v=1}=1$ so that the angular distribution (3.10) reduces to that given in Eq. (3.2) for the massless-quark case. In Fig. 7, we have plotted $B_1(v)$ and $B_0(v)$ as a function of the velocity. The QCD correction is small except for large and small values of v. For small values of v, the QCD correction grows like inverse powers of v,

$$1+\frac{\tilde{\alpha}}{\pi}P\to 1+\frac{\tilde{\alpha}\pi}{2v}, \tag{3.11a}$$

$$B_1(v)\to B_0(v)\left[1+O\left(\frac{\tilde{\alpha}}{v}\right)\right], \tag{3.11b}$$

and hence the perturbative approximation breaks down. (This phenomenon is well understood in

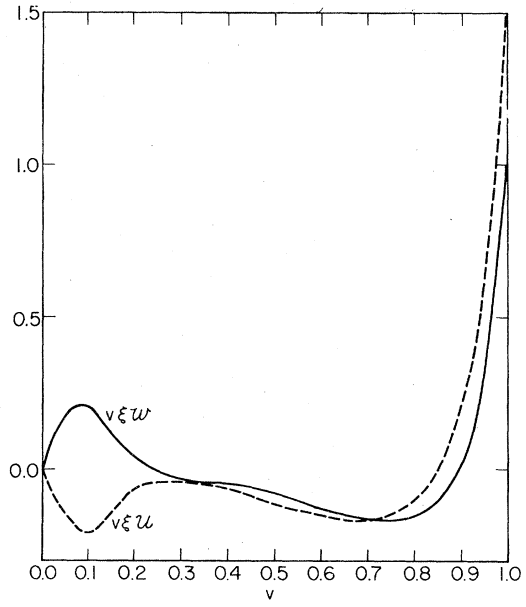

FIG. 6. The function $v\xi\mathfrak{w}$ in Eq. (3.8) and the function $v\xi\mathfrak{u}$ in Eq. (3.14). The solid curve is the function $v\xi\mathfrak{w}$ (the ordinary cross-section case) and the dashed curve is the function $v\xi\mathfrak{u}$ (the energy-weighted cross-section case). The curves for the region $0\le v\le 0.1$ are indicative at best. They are based on values at only two points, viz, $v=0$ and $v=0.1$.

TABLE I. Values of vP, $\xi\mathfrak{W}$, and $\xi\mathfrak{U}$ for different values of the velocity v.

v	0	0.1	0.2	0.3	0.4	0.5	0.6	0.7	0.8	0.9	1
vP	4.94	4.61	4.27	3.90	3.51	3.10	2.68	2.23	1.75	1.26	0.75
$\xi\mathfrak{W}$	0	2.10	0.19	−0.09	−0.09	−0.12	−0.21	−0.22	−0.20	0.03	1
$\xi\mathfrak{U}$	0	−2.09	−0.28	−0.10	−0.16	−0.23	−0.25	−0.24	−0.12	0.27	1.50

QED).[11] For our purpose, we should avoid small v regions by considering only values of v such that $\alpha_c/v < 1$. We note that for $v \gtrsim \alpha_c$, the QCD effect gives only a small correction to the coefficient $B_1(v)$. In terms of mass and energy, this means $B_1(m, s)$ is close to that given by $B_0(m, s)$ once we are at energies above the continuum threshold. The QCD correction remains small until we get to energies much bigger than the quark mass involved, say, $E_{\text{c.m.}} \gtrsim 5m_q$.

$B_1(m, s)$ for the charmed and the b quarks are shown in Fig. 8.

Alternatively, it may be more convenient for experimentalists to measure the angular distribution of the energy-weighted cross section.[12] This is defined by

$$\frac{1}{\sigma_0}\frac{d\Sigma}{d\cos\theta} = \sum_j \frac{1}{\sigma_0}\int\int dE_j\,\frac{E_j}{W}\frac{d^2\sigma}{dE_j d\cos\theta_j}\,d\cos\theta_j\,\delta(\cos\theta_j - \cos\theta)\,, \tag{3.12}$$

where the summation is over all hadrons. For the perturbative QCD correction term, the sum j converts to a sum over quarks and gluons. Integrating Eqs. (3.3) and (3.4) with the appropriate energy weights, we obtain (see Sec. IV)

$$\frac{1}{\sigma_0}\frac{d\Sigma}{d\cos\theta} = \frac{3}{8}\left(1+\frac{\tilde\alpha}{\pi}P\right)\frac{v}{2}\left[(3-v^2)(1+\cos^2\theta) + \xi(1-3\cos^2\theta)\left(1+\frac{\tilde\alpha}{\pi}\mathfrak{U}\right)\right], \tag{3.13}$$

where

$$\begin{aligned} v\xi\mathfrak{U} &= \xi(1-3\xi)\left[L\left(\frac{1+v}{2}\right) - L\left(\frac{1-v}{2}\right)\right] + \frac{\tilde{\mathfrak{M}}}{2} + \frac{3}{2}v + v\xi\left[\frac{3}{2+\xi} + \frac{7}{3} - \frac{\xi}{12} + \frac{\xi^2}{8}\right] \\ &\quad + \frac{\xi}{2}\ln\left(\frac{1+v}{1-v}\right)\left[-\sqrt{\xi}(1+\xi)\ln\left(\frac{2+\sqrt{\xi}}{2-\sqrt{\xi}}\right) + (3\xi-1)\ln\left(\frac{4}{4-\xi}\right) - \frac{1}{4}\frac{(4-\xi)^2}{2+\xi} - 3 - \frac{5}{4}\xi + \frac{\xi^3}{8}\right], \\ \tilde{\mathfrak{M}} &= \sqrt{\xi}\left[\mathfrak{M}_1(\sqrt{\xi}, v) - \mathfrak{M}_1(-\sqrt{\xi}, v)\right], \end{aligned} \tag{3.14}$$

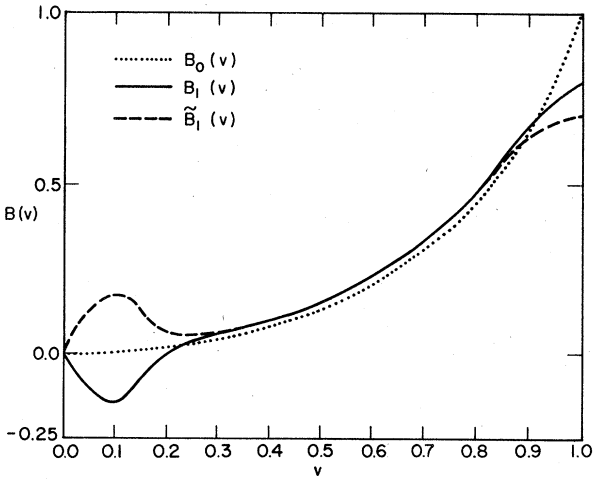

FIG. 7. The coefficients $B_0(v)$ (dotted curve), $B_1(v)$ given in Eq. (3.10) (solid curve), and $\tilde{B}_1(v)$ given in Eq. (3.15) (dashed curve). We have used $\tilde\alpha/\pi = 0.1$. Note that for values of v such that $\alpha_c/v > 1$ the perturbative approximation actually breaks down.

where $\mathfrak{M}_1$ is given by Eq. (3.9). If we rewrite Eq. (3.13) as

$$\frac{1}{\sigma_0}\frac{d\Sigma}{d\cos\theta} \propto 1 + \tilde B_1(v)\cos^2\theta,$$

then

$$\tilde B_1(v) = \frac{v^2}{2-v^2}\left(1 - \frac{\tilde\alpha}{\pi}\xi\mathfrak{U}(v)\,\frac{3-v^2}{v^2(2-v^2)}\right). \tag{3.15}$$

The functions $v\xi\mathfrak{U}$ is plotted in Fig. 6 while the coefficient $\tilde B_1(v)$ is plotted in Fig. 7. Values of $\xi\mathfrak{U}$ are given in Table I. We observe that as $v \to 1$ (or as quark mass is taken to be zero), Eq. (3.13) becomes[12]

$$\begin{aligned} \frac{1}{\sigma_0}\frac{d\Sigma}{d\cos\theta} &= \tfrac{3}{8}\left[\left(1+\tfrac{3}{4}\frac{\tilde\alpha}{\pi}\right)(1+\cos^2\theta) + \tfrac{3}{4}\frac{\tilde\alpha}{\pi}\,(1-3\cos^2\theta)\right] \\ &\propto 1 + \left(1 - \frac{3\tilde\alpha}{\pi}\right)\cos^2\theta\,. \end{aligned} \tag{3.16}$$

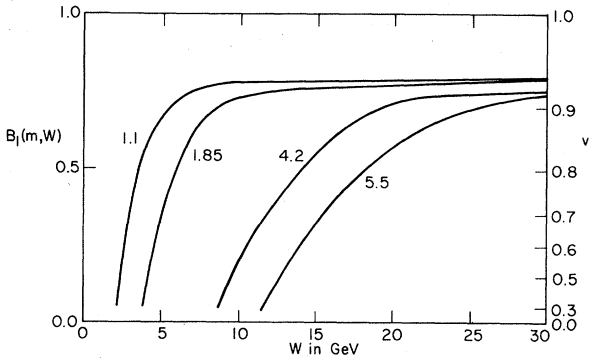

FIG. 8. The coefficient $B_1(m, W)$ as a function of quark mass m (in GeV) and the center-of-mass energy W. The value of the velocity is plotted on the y axis at the right-hand side. $\tilde{\alpha}/\pi = 0.1$.

In Fig. 9, σ_{tot} and $\tilde{B}_1(m, W)$ are plotted for the b-quark case. For comparison, we also include the zeroth-order coefficient $B_0(m, W) = \tilde{B}_0(m, W)$ for $m_q = 4.2$ GeV. Figure 10 shows σ_{tot} and $\tilde{B}_1(m, W)$ for the charmed-quark case.

For our numerical work we have used $\tilde{\alpha}/\pi = 0.1$, or $\alpha_c = 0.24$. To be more accurate, we should use a running coupling constant with a determined Λ in $\alpha_c \propto [\ln(W^2/\Lambda^2)]^{-1}$. Properties of the renormalization group and asymptotic freedom do not allow us an accurate determination of the value of Λ at present energies from other experiments (such as deep-inelastic scatterings) without the evaluation of higher-order QCD corrections to $B(v)$ or $\tilde{B}(v)$.[13] Hence, to determine α_c (or Λ) that comes in $B(v)$

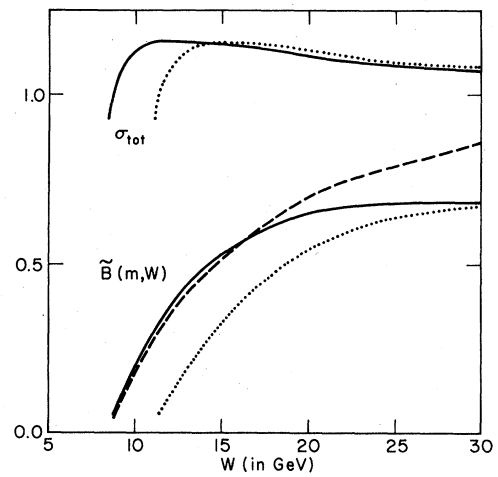

FIG. 9. The b-quark case. The total cross section (normalized to σ_0) to order α_c and the coefficient $B_1(m, W)$. The solid curves are for quark mass $m = 4.2$ GeV. The dotted curves are for quark mass $m = 5.5$ GeV. The dashed curve is $\tilde{B}_0(m, W)$ for $m = 4.2$ GeV. It is included for comparison.

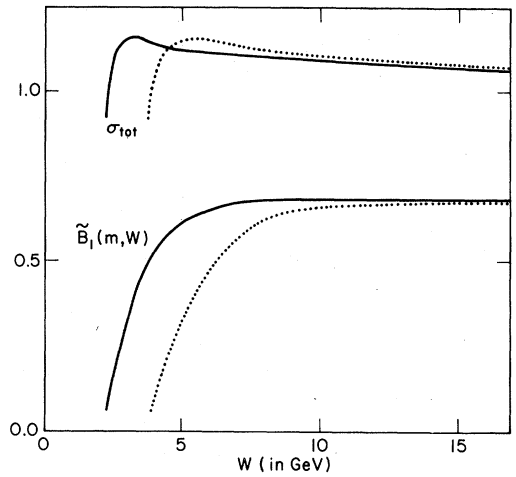

FIG. 10. The charmed-quark case. The solid curves are for $m = 1.1$ GeV. The dotted curves are for $m = 1.85$ GeV. σ_{tot} is normalized to σ_0.

or $\tilde{B}(v)$, it is best to measure the angular distribution of the quark jet for light quarks. Data (for jet angular distributions) available from SPEAR and DORIS[14] seem to indicate α_c to be smaller than the value we have used.

We end this section with three remarks:

(1) Depending on the type of detector used, either $d\sigma/d\cos\theta_1$ or $d\Sigma/d\cos\theta$ is the better quantity to be measured experimentally. Hence we have evaluated both. In fact, one can go back to the differential cross section (3.3) and consider other quantities that are measurable in experiments. An example is the energy correlation for the massive-quark gluon bremsstrahlung process.

(2) We observe that the coefficient of the $(1 + \cos^2\theta)$ term of both $d\sigma/d\cos\theta_1$ and $d\Sigma/d\cos\theta$ is $\frac{3}{8}$ times the total hadronic cross section. Hence $d\sigma/d\cos\theta_1$ or $d\Sigma/d\cos\theta$ provides a clear measurement of the total hadronic cross section. In fact, both σ_{tot} and $\tilde{B}(m, W)$ [or $B(m, W)$] are determined by measuring $d\Sigma/d\cos\theta$ (or $d\sigma/d\cos\theta$) at two different angles at a given c.m. energy W. This method of determining σ_{tot} has the advantage of avoiding the forward and backward cones where two-photon events dominate at high energies.

(3) Our method provides an accurate way to measure heavy-quark masses. Essentially there are only two sources of error in these measurements. The relatively minor source comes from QCD corrections. An error ~20% in α_c will cause an error ~1% in the coefficient of $\cos\theta$. More serious is the angular uncertainty. For example, an error of ~5° at $E_{\text{c.m.}} = 16$ GeV, $\theta = 30°$ [according to our estimate using Eq. (3.10)] will translate into an error ~6% for the b-quark mass. Of course, better accuracy can be achieved by accumulating measurements at different $E_{\text{c.m.}}$ and different angle

θ.

IV. DERIVATION OF THE LEADING-ORDER PERTURBATIVE QCD CORRECTION

We will devote this section to present the detailed calculation of the QCD processes. Some necessary integrals are given in the Appendix. Let us first consider the gluon-bremsstrahlung diagrams. We average over the initial e^+e^- polarizations and sum over the final-state polarizations to obtain the matrix element squared (we perform our calculations in Feynman gauge):

$$|M|^2=\frac{2}{yz}[(1-y)^2(1+\cos^2\theta_1)+(1-z)^2(1+\cos^2\theta_2)]$$
$$-\xi\left\{\frac{4}{y}+\frac{4}{z}+\left(\frac{1}{y}-\frac{1}{z}\right)^2+\left[\frac{2+(1-y)^2}{yz}+\left(\frac{1-y}{y}\right)^2\right]\cos^2\theta_1+\left[\frac{2+(1-z)^2}{yz}+\left(\frac{1-z}{z}\right)^2\right]\cos^2\theta_2-\frac{(y+z)^2}{yz}\cos^2\theta_3\right\}$$
$$-\xi^2\left[\left(\frac{1}{y}+\frac{1}{z}\right)^2-\left(\frac{1}{yz}+\frac{1}{y^2}\right)\cos^2\theta_1-\left(\frac{1}{yz}+\frac{1}{z^2}\right)\cos^2\theta_2\right], \tag{4.1}$$

where $\xi=4m^2/s$, $y=1-x_1=1-2E_1/W$, $z=1-x_2=1-2E_2/W$, and $\theta_1,\theta_2,\theta_3$ are the angles made by the outgoing quark, antiquark, and gluon, respective to the electron direction. To ameliorate the infrared problem, we introduce a small mass λ for the gluon. λ shall be taken to be zero after the cancellation of the infrared divergences between the gluon-bremsstrahlung and the radiative-correction diagrams. Terms that will vanish in the limit $\lambda\to 0$ are neglected.

The three-body phase space can be written as

$$\frac{d^3p_1}{E_1}\frac{d^3p_2}{E_2}\frac{d^3p_3}{E_3}\delta^4(p_1+p_2+p_3-p_{e^+}-p_{e^-})=dE_1dE_2d\Omega_1d\cos\eta_{12}d\phi_{12}\delta\left(\cos\eta_{12}-\frac{s-2W(E_1+E_2)+2E_1E_2+2m^2-\lambda^2}{2|\vec{p}_1||\vec{p}_2|}\right), \tag{4.2}$$

where Ω_1 is the solid angle of the quark and (η_{12},ϕ_{12}) is the orientation of the antiquark relative to the quark. Similarly, we can introduce other Ω_i and (η_{ij},ϕ_{ij}) and write Eq. (4.1) in terms of them. To obtain Eq. (3.3), we have to express the angles θ_2 and θ_3 in terms of θ_1,

$$\cos\theta_2=\cos\theta_1\cos\eta_{12}+\sin\theta_1\sin\eta_{12}\cos\phi_{12}.$$

Integrating over the azimuthal angle ϕ_{12}, we obtain

$$\cos^2\theta_2\to\tfrac{1}{4}(1+\cos^2\theta_1)+(\tfrac{1}{2}\sin^2\eta_{12}-\tfrac{1}{4})(1-3\cos^2\theta_1), \tag{4.3}$$

and similarly for θ_3. From the δ function in Eq. (4.2), we obtain

$$\sin^2\eta_{12}=\frac{4yz(1-y-z)-\xi(y+z)^2}{[(1-y)^2-\xi][(1-z)^2-\xi]}. \tag{4.4a}$$

Similarly,

$$\sin^2\eta_{13}=\frac{4yz(1-y-z)-\xi(y+z)^2}{[(1-y)^2-\xi](y+z)^2}. \tag{4.4b}$$

Using Eqs. (4.1), (4.2), (4.3), and (4.4), we obtain Eq. (3.3) from the following differential cross section,

$$d\sigma_i=\frac{d^3p_1}{(2\pi)^32E_1}\frac{d^3p_2}{(2\pi)^32E_2}\frac{d^3p_3}{(2\pi)^32E_3}$$
$$\times(2\pi)^4\delta^4(p_1+p_2+p_3-p_{e^+}-p_{e^-})$$
$$\times\frac{1}{2W^2}3(4\pi)^3\alpha^2\tilde{\alpha}e_i^2\frac{|M|^2}{W^2}. \tag{4.5}$$

Equation (3.4) follows by introducing the angle η_{23} in Eq. (4.2).

To obtain $d\sigma/d\cos\theta_q$ and $d\Sigma/d\cos\theta$, we must first obtain the boundary of the phase space. This follows from the requirement that $|\cos\eta|\le 1$. In terms of the variables y and z, this constraint implies (see Fig. 11)

$$yz(y+z-1)+\tfrac{1}{4}\xi(y+z)^2$$
$$-\Lambda(\xi+yz+y+z-1)+\Lambda^2\le 1, \tag{4.6}$$

where $\Lambda=\lambda^2/W^2$.

It turns out that the following variables

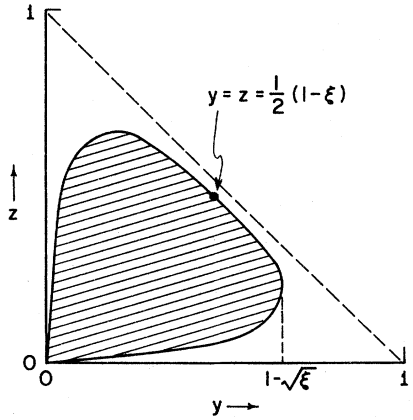

FIG. 11. The phase space for the gluon bremsstrahlung for the massive-quark and massless-gluon case. The triangle ($y>0$, $z>0$, $y+z\le 1$) is the phase-space boundary for the massless-quark case.

$$w=-y+z, \quad x=y+z$$

are more convenient. In terms of them, the bounds due to phase space become

$$1-\xi \geq x \geq 2\Lambda^{1/2},$$

$$|w| \leq x\left[\left(1-\frac{4\Lambda}{x^2}\right)\left(1-\frac{\xi}{1-x+\Lambda}\right)\right]^{1/2}.$$

Figure 11 illustrates the phase-space boundary with $\Lambda=0$. Integrating the differential cross section (3.3) over the energies (integrals that occur here are given in the Appendix), we obtain, for the real-gluon emission process,

$$\frac{1}{\sigma}\frac{d\sigma_R}{d\cos\theta_q}=\frac{\alpha_c}{64\pi}\left[A_1(1+\cos^2\theta_q)+\left(A_2+\frac{P_1}{\sqrt{\xi}}\right)(1-3\cos^2\theta_q)\right], \tag{4.7}$$

where

$$A_{1,2}=\int\int dx\,dw\,\mathfrak{A}_{1,2}, \tag{4.8}$$

$$P_1=8\int\int dx\,dw\sqrt{\xi}\,\mathfrak{A}_3 G, \tag{4.9}$$

and $\mathfrak{A}_1$, $\mathfrak{A}_2$, $\mathfrak{A}_3$, and G are given in Eq. (3.3). The energy-weighted cross section for real gluon emission is given by

$$\frac{1}{\sigma_0}\frac{d\Sigma_R}{d\cos\theta}=\frac{1}{\sigma_0}\sum_{i=0}^{3}\left(\int\int dx\,dw\,x_i\frac{d\sigma}{dx\,dw\,d\cos\theta_i}\right)_{\theta_i=\theta}$$

$$=\frac{\alpha_c}{64\pi}[A_1(1+\cos^2\theta)+(A_2+P_2+C)(1-3\cos^2\theta)], \tag{4.10}$$

where

$$P_2=8\int\int dx\,dw\,(1-y)\mathfrak{A}_3 G, \tag{4.11}$$

$$C=8\int\int dx\,dw\,\tfrac{1}{2}(y+z)\mathfrak{A}_3\mathfrak{C}, \tag{4.12}$$

and $\mathfrak{C}$ is given in Eq. (3.4). We note that A_1 and A_2 involve infrared divergent terms while P_1, P_2, and C are finite. If we introduce

$$2\tilde{B}_\pm=P_2\pm P_1, \tag{4.13}$$

then $\tilde{B}_+=\tilde{B}_-(\sqrt{\xi}\to-\sqrt{\xi})$. Hence it suffices to evaluate A_1, A_2, C, and $\tilde{B}_+$. With the aid of the integrals given in the Appendix we obtain $(1-\xi=v^2)$,

$$A_1=(2+\xi)[16(2-\xi)D_1-8\xi D_2-32I_1]+16(2I_2-I_5), \tag{4.14}$$

where

$$16(2-\xi)D_1-8\xi D_2-32I_1=16\ln(\Lambda^{1/2})\left[2v-(2-\xi)\ln\frac{1+v}{1-v}\right]$$

$$+16(2-\xi)\left[L\left(\frac{1+v}{2}\right)-L\left(\frac{1-v}{2}\right)+\frac{3}{2}L\left(-\frac{2v}{1-v}\right)-\frac{3}{2}L\left(\frac{2v}{1+v}\right)\right]$$

$$+64v\left(1-\ln\frac{2v}{\sqrt{\xi}}\right)+16\ln\left(\frac{1+v}{1-v}\right)\left[(2-\xi)\ln\left(\frac{2v^2}{\sqrt{\xi}}\right)+1\right]$$

and

$$2I_2-I_5=v\left(-\frac{5}{2}+\frac{\xi}{4}\right)+\ln\left(\frac{1+v}{1-v}\right)\left(1+\frac{\xi^2}{8}\right).$$

$L(x)$ is the Spence function

$$L(x)=-\int_0^x dt\frac{\ln|1-t|}{t},$$

and

$$A_2=\xi[16(2-\xi)D_1-8\xi D_2-32I_1]. \tag{4.15}$$

The integral C can also be evaluated in a straightforward manner with the aid of the integrals given in the Appendix,

$$C=-8(4\xi-\xi^2)I_1+16\xi I_2+8\xi^2 I_3+16I_4-16I_5$$

$$=v(16+\tfrac{52}{3}\xi-\tfrac{22}{3}\xi^2+2\xi^3)+\ln\left(\frac{1+v}{1-v}\right)(-24\xi+12\xi^2-3\xi^3+\xi^4). \tag{4.16}$$

The evaluation of $\tilde{B}_+$ is more tedious. With the aid of the integrals given in the Appendix we obtain $[g=(1-\xi^{1/2})^{1/2}]$

$$\begin{aligned}\tilde{B}_+ &= -2\xi^3 K_1 + \xi^2(2-\sqrt{\xi})^2 K_2 + \xi^{3/2}(8 - 12\sqrt{\xi} + 4\xi + \xi^{3/2})K_3 - 8g\xi^{3/2}(1-\xi^{1/2})K_4 + 8\sqrt{\xi}\,[\sqrt{\xi}(3\xi-1) - \xi(1+\xi)]L_1 \\ &\quad + \xi^2(6 - 8\sqrt{\xi} + \xi)L_2 + \frac{\xi^2(2-\sqrt{\xi})(-2+7\sqrt{\xi}-2\xi)}{1-\sqrt{\xi}} L_3 - 2g\xi^2(1-\sqrt{\xi})L_4 + 2\xi^2(2-\xi)L_5 - \frac{2\xi^2(2-\sqrt{\xi})^2}{1-\sqrt{\xi}} L_6 \\ &= 8\sqrt{\xi}\,[\sqrt{\xi}(3\xi-1) - \xi(1+\xi)]S + v(4 + 12\xi + 3\xi^2 + 8\sqrt{\xi} - 24\xi^{3/2}) \\ &\quad + \frac{\xi}{2}\ln\left(\frac{1+v}{1-v}\right)\left[16(-1 + 3\xi - \sqrt{\xi} - \xi^{3/2})\ln\frac{2}{2-\sqrt{\xi}} + 24\xi^{1/2} - 8\xi^{3/2} - 22\xi + 3\xi^2\right], \end{aligned} \tag{4.17}$$

where the function S is given in the Appendix. From the definition (4.13), we obtain

$$\begin{aligned}\frac{1}{16}\frac{1}{\sqrt{\xi}} P_1 &= \tfrac{1}{2}\{[(3\xi^{3/2} - \xi^{1/2} - \xi - \xi^2)S] + (\sqrt{\xi} \to -\sqrt{\xi})\} + v - 3\xi v \\ &\quad + \frac{\xi}{2}\ln\left(\frac{1+v}{1-v}\right)\left[\frac{1}{\sqrt{\xi}}(-1+3\xi)\ln\left(\frac{2+\sqrt{\xi}}{2-\sqrt{\xi}}\right) - (1+\xi)\ln\left(\frac{4}{4-\xi}\right) + 3 - \xi\right], \end{aligned} \tag{4.18}$$

$$\begin{aligned}\tfrac{1}{16} P_2 &= \tfrac{1}{2}\{[3\xi^2 - \xi - \xi^{3/2} - \xi^{5/2})S] + (\sqrt{\xi} \to -\sqrt{\xi})\} + v(\tfrac{1}{2} + \tfrac{3}{2}\xi + \tfrac{3}{8}\xi^2) \\ &\quad + \frac{\xi}{2}\ln\left(\frac{1+v}{1-v}\right)\left[-\xi^{1/2}(1+\xi)\ln\left(\frac{2+\sqrt{\xi}}{2-\sqrt{\xi}}\right) + (-1+3\xi)\ln\left(\frac{4}{4-\xi}\right) - \tfrac{11}{4}\xi + \tfrac{3}{8}\xi^2\right]. \end{aligned} \tag{4.19}$$

From Eqs. (4.14), (4.15), (4.16), (4.18), and (4.19), we obtain the cross sections for the gluon bremsstrahlung process. To obtain the physical cross sections $(1/\sigma_0)d\sigma/d\cos\theta_q$ and $(1/\sigma_0)d\Sigma/d\cos\theta$, we must include the radiative correction diagrams.

The evaluation of the radiative-correction diagram is straightforward with the introduction of the electric and magnetic form factors F_1 and F_2. They are given in standard textbooks (see, e.g., Ref. 10),

$$\begin{aligned}F_1(v) &= 1 - \frac{\alpha_s}{2\pi} f_1, \\ f_1 &= 2(-\tfrac{1}{2}\ln\Lambda + \tfrac{1}{2}\ln\xi - 1)\left[\frac{1+v^2}{2v}\ln\left(\frac{1+v}{1-v}\right) - 1\right] + 2\ln 2 \\ &\quad + \frac{1+v^2}{2v}\left\{-\pi^2 + \tfrac{1}{2}\left[\ln\left(\frac{1-v}{2}\right)\right]^2 - \tfrac{1}{2}\left[\ln\left(\frac{1+v}{2}\right)\right]^2 - 2\ln 2\ln\left(\frac{1+v}{1-v}\right) + 4L(v) - L(v^2) - L\left(\frac{1+v}{2}\right) + L\left(\frac{1-v}{2}\right)\right\}, \end{aligned} \tag{4.20}$$

and

$$F_2(v) = \frac{\alpha_s}{2\pi}\frac{\xi}{2v}\ln\left(\frac{1+v}{1-v}\right). \tag{4.21}$$

This gives, including the zeroth-order diagram,

$$\begin{aligned}\frac{1}{\sigma_0}\frac{d\sigma_V}{d\cos\theta} &= \tfrac{3}{8}v\left\{(1+\cos^2\theta)\left[(1+\tfrac{1}{2}\xi)\left(1 - \frac{\tilde{\alpha}}{\pi}f_1\right) - 4F_2\right] + (1 - 3\cos^2\theta)\left[\frac{\xi}{2}\left(1 - \frac{\tilde{\alpha}}{\pi}f_1\right) - \tfrac{4}{3}F_2\right]\right\} \\ &= \frac{1}{\sigma_0}\frac{d\Sigma_V}{d\cos\theta}, \end{aligned} \tag{4.22}$$

since for two-body final state $\theta = \theta_1$. We have included factors of 3 and 4 for the zeroth-order and the radiative processes, respectively, coming from color summation. The subscript V in Eq. (4.22) denotes virtual-gluon emission. Combining Eqs. (4.7) and (4.22), we obtain Eq. (3.5) where

$$\begin{aligned}P = \frac{1}{v(3-v^2)}\Bigg\{&(3-v^2)(1+v^2)\left[\frac{\pi^2}{6} + \ln\left(\frac{1+v}{2}\right)\ln\left(\frac{1+v}{1-v}\right) - 4L(v)\right. \\ &\left. + L(v^2) + 2L\left(\frac{1-v}{1+v}\right) + 2L\left(\frac{1+v}{2}\right) - 2L\left(\frac{1-v}{2}\right)\right] \\ &+ \ln\left(\frac{1+v}{1-v}\right)\left[\tfrac{11}{8}(3-v^2)(1+v^2) + \tfrac{1}{2}v^4 - 3v(3-v^2)\right] \\ &+ 6v(3-v^2)\ln\left(\frac{1+v}{2}\right) - 4v(3-v^2)\ln v + \tfrac{3}{4}v(5-3v^2)\Bigg\}. \end{aligned} \tag{4.23}$$

Integrating over the angle θ, we have

$$\frac{\sigma}{\sigma_0}=\left(1+\frac{\tilde{\alpha}}{\pi}P(v)\right)\frac{v}{2}(3-v^2), \tag{3.6}$$

which agrees with the result given by Schwinger.[10] The form for P in Eq. (4.23) is obtained by using the following Spence-function identity, in addition to the standard ones,[15]

$$L(x)-L(-x)=-L\left(\frac{2}{1+x}\right)+L\left(\frac{2x}{1+x}\right)+\frac{\pi^2}{4}.$$

Similarly the energy-weighted cross section (3.14) can be obtained by adding Eqs. (4.10) and (4.22).

ACKNOWLEDGMENTS

Two of us (G.G. and Y.J.N.) thank K. Gottfried, T. Kinoshita, and T. M. Yan for the hospitality extended by the theory group at Cornell where part of this work was done. The work of G. G. and S.-H. H. T. was supported in part by the National Science Foundation and that of Y. J. N. was supported in part by the Department of Energy.

APPENDIX

Here we present the integrals that occur in Sec. IV. In evaluating A_1, A_2, and C the following integrals are necessary. The limits of integration are

$$w=\pm x\left[\left(1-\frac{4\Lambda}{x^2}\right)\left(1-\frac{\xi}{1-x+\Lambda}\right)\right]^{1/2}$$

and

$$1-\xi\geq x\geq 2\Lambda^{1/2}.$$

The integrals are

$$D_1=\int\int dx\,dw\,\frac{1}{4yz}$$
$$=(-\ln\Lambda^{1/2}-\tfrac{1}{2}\ln\xi+2\ln v+\ln 2)\ln\left(\frac{1+v}{1-v}\right)$$
$$-L\left(\frac{1-v}{2}\right)+L\left(\frac{1+v}{2}\right)-\tfrac{3}{2}L\left(\frac{2v}{1+v}\right)+\tfrac{3}{2}L\left(-\frac{2v}{1-v}\right),$$

$$D_2=\int\int dx\,dw\,\tfrac{1}{4}\left(\frac{1}{y^2}+\frac{1}{z^2}\right)$$
$$=-\frac{4v}{\xi}(\ln\Lambda^{1/2}+\ln\xi-2\ln v-2\ln 2+1)$$
$$+\left(2-\frac{6}{\xi}\right)\ln\frac{1+v}{1-v},$$

$$I_1=\int\int dx\,dw\,\frac{1}{w+x}=-v+(1-\tfrac{1}{2}\xi)\ln\frac{1+v}{1-v},$$

$$I_2=\int\int dx\,dw\,\frac{x}{w+x}=v(-\tfrac{3}{4}+\tfrac{3}{8}\xi)+(\tfrac{1}{2}-\tfrac{1}{2}\xi+\tfrac{3}{16}\xi^2)$$
$$\times\ln\frac{1+v}{1-v},$$

$$I_3=\int\int dx\,dw\,\frac{x}{(w+x)^2}$$
$$=v\left(\frac{2}{3}\frac{1}{\xi}-\frac{2}{3}+\frac{\xi}{4}\right)+\left(-\frac{\xi}{4}+\frac{\xi^2}{8}\right)\ln\frac{1+v}{1-v},$$

$$I_4=\int\int dx\,dw\,\frac{1}{x}=2v-\xi\ln\frac{1+v}{1-v},$$

$$I_5=\int\int dx\,dw(1)=v(1+\tfrac{1}{2}\xi)+(-\xi+\tfrac{1}{4}\xi^2)\ln\frac{1+v}{1-v}.$$

In evaluating $\tilde{B}_+$ the following integrals occur. The w integration is straightforward. For the x integration a change of variable

$$x\to u\equiv\left(1-\frac{\xi}{1-x}\right)^{1/2}$$

is helpful. For the w integration, the limits of integration are $\pm xu$,

$$\int dw\,\frac{1}{(w+x)^2}=\frac{1}{x}\left(\frac{1}{1-u}-\frac{1}{1+u}\right),$$

$$\int dw\,\frac{1}{w+x}=J_1,$$

$$\int dw\,\frac{1}{w-x+2g^2}=2J_2-J_1,$$

where

$$g^2=1-\sqrt{\xi},$$

$$J_1=\ln\left|\frac{1+u}{1-u}\right|,$$

$$J_2=\ln\left|\frac{u+g^2}{u-g^2}\right|.$$

Then we encounter the following integrals ($v=\sqrt{1-\xi}$):

$$K_1=\int_0^v du\,\frac{1}{(1+u)^3}-(v\to -v)=\frac{2v}{\xi^2},$$

$$K_2=\int_0^v du\,\frac{1}{(1+u)^2}-(v\to -v)=\frac{2v}{\xi},$$

$$K_3=\int_0^v du\,\frac{1}{(1+u)}-(v\to -v)=\ln\frac{1+v}{1-v},$$

$$K_4=\int_0^v du\,\frac{1}{u+g}-(v\to -v)=\ln\left|\frac{v+g}{v-g}\right|,$$

$$L_1=\int_0^v du\left(\frac{1}{1+u}-\frac{1}{g+u}\right)(J_2-J_1)-(v\to -v)$$
$$=\ln\left(\frac{1+v}{1-v}\right)\ln\left(\frac{2}{1+g^2}\right)+S,$$

where

$$S = L\left(\frac{1-v}{2}\right) - L\left(\frac{1+v}{2}\right) + L\left(\frac{1+v}{1+g^2}\right) - L\left(\frac{1-v}{1+g^2}\right) - L\left(\frac{1+v}{1-g^2}\right) + L\left(\frac{1-v}{1-g^2}\right) + L\left(+\frac{g-v}{g+g^2}\right)$$
$$- L\left(\frac{v+g}{g+g^2}\right) - L\left(+\frac{g-v}{g-g^2}\right) + L\left(\frac{v+g}{g-g^2}\right) - L\left(\frac{g-v}{1+g}\right) + L\left(\frac{v+g}{1+g}\right) + L\left(\frac{v-g}{1-g}\right) - L\left(\frac{v+g}{g-1}\right),$$

$$L_2 = \int_0^v du \frac{1}{(1+u)^2} J_1 - (v \to -v) = \frac{2v}{\xi} - \left(\frac{2-\xi}{\xi}\right) \ln \frac{1+v}{1-v},$$

$$L_3 = \int_0^v du \frac{1}{(1+u)^2} J_2 - (v \to -v) = \ln\left(\frac{1+v}{1-v}\right)\left(-\frac{1}{\xi} + \frac{2}{2-\sqrt{\xi}} - \frac{1}{\sqrt{\xi}(2-\sqrt{\xi})}\right),$$

$$L_4 = \int_0^v du \frac{1}{(g+u)^2}(J_2 - J_1) - (v \to -v) = -\frac{4}{\sqrt{\xi}} \ln \frac{v+g}{v-g} + \frac{2g}{\sqrt{\xi}} \ln \frac{1+v}{1-v},$$

$$L_5 = \int_0^v du \frac{1}{(1+u)^3} J_1 - (v \to -v) = \frac{3v - v^3}{2\xi^2} + \left(\tfrac{1}{4} + \frac{1}{\xi} - \frac{2}{\xi^2}\right) \ln \frac{1+v}{1-v},$$

$$L_6 = \int_0^v du \frac{1}{(1+u)^3} J_2 - (v \to -v)$$
$$= -\frac{2v(1-\sqrt{\xi})}{2\xi^{3/2} - \xi^2} + \ln\left(\frac{1+v}{1-v}\right)\left(-\frac{1}{\xi^2} + \frac{1-\sqrt{\xi}+\xi}{\xi(2-\sqrt{\xi})^2}\right).$$

---

*Physique Mathématique et Théorique, équipe de recherche associée au C.N.R.S.

[1]In our discussion, we shall assume exact quark confinement. Our position on the recent experiment by G. S. LaRue *et al.* [Phys. Rev. Lett. 42, 142 (1979)] is that, if their experiment is confirmed, it is due to the existence of a heavy exotic quark. Either the quark is integrally charged, or it is in some higher color representation. Both can give fractionally charged hadrons (i.e., color singlets).

[2]See, e.g., G. Bhanot and S. Rudaz, Phys. Lett. 78B, 119 (1978); E. Eichten, K. Gottfried, T. Kinoshita, K. Lane, and T. M. Yan, Phys. Rev. D 17, 3090 (1978); 21, 313 (E) (1980); 21, 203 (1980).
Of course the quark masses they use may have nothing to do with the quark masses in the QCD Lagrangian.

[3]E. C. Poggio, H. R. Quinn, and S. Weinberg, Phys. Rev. D 13, 1958 (1976).

[4]R. Shankar, Phys. Rev. D 15, 755 (1977); E. Floratos, S. Narison, and E. deRafael, Nucl. Phys. B155, 115 (1979); T. Hagiwara and A. I. Sanda, Brandeis Report No. COO-2232B-165, 1979 (unpublished); M. Greco, G. Penso, and Y. Srivastava, Report No. LNF-78/49, 1978 (unpublished).

[5]For example, S. Weinberg, in *Festschrift for I. I. Rabi*, edited by L. Motz (N. Y. Academy of Sciences, N. Y., 1977).

[6]G. 't Hooft, Nucl. Phys. B75, 461 (1974); M. B. Einhorn, Phys. Rev. D 14, 3451 (1976); C. G. Callan, N. Coote, and D. J. Gross, *ibid.* 13, 1649 (1976).

[7]H. Georgi and H. D. Politzer, Phys. Rev. D 14, 1829 (1976); A. De Rújula and H. Georgi, *ibid.* 13, 1296 (1976).

[8]For example, J. Ellis, M. K. Gaillard, and G. G. Ross, Nucl. Phys. B111, 253 (1976); B130, 516(E) (1977); T. A. DeGrand, Y. J. Ng, and S.-H. H. Tye, Phys. Rev. D 16, 3251 (1977).

[9]This agrees with the formula previously derived by B. L. Ioffe and A. V. Smilga, Report No. ITEP-69, 1978 (unpublished).

[10]J. Schwinger, *Particles, Sources and Fields* (Addison-Wesley, New York, 1973), Vol. II, Sec. 5.4.

[11]See, e.g., Refs. 3 and 10; T. Appelquist and H. D. Politzer, Phys. Rev. D 12, 1404 (1975).

[12]C. L. Basham, L. S. Brown, S. D. Ellis, and S. T. Love, Phys. Rev. D 17, 2298 (1978); Phys. Rev. Lett. 41, 1585 (1978).

[13]See, e.g., W. A. Bardeen, A. J. Buras, D. W. Duke, and T. Muta, Phys. Rev. D 18, 3998 (1978).

[14]G. Hanson *et al.*, Phys. Rev. Lett. 35, 1609 (1975); PLUTO Collaboration, Ch. Berger *et al.*, Phys. Lett. B76, 243 (1978); B78, 176 (1978).

[15]K. Mitchell, Philos. Mag. 40, 351 (1949); L. DeRaad, Jr. and Y. J. Ng, Phys. Rev. D 10, 3440 (1974).